Eur Biophys J (2012) 41:801–813
DOI 10.1007/s00249-012-0841-5

ORIGINAL PAPER

EBSA
Biophysics in Europe

The role of G-domain orientation and nucleotide state on the Ras isoform-specific membrane interaction

Shobhna Kapoor · Katrin Weise · Mirko Erlkamp · Gemma Triola · Herbert Waldmann · Roland Winter

Received: 16 May 2012 / Revised: 26 June 2012 / Accepted: 10 July 2012 / Published online: 1 August 2012

Abstract Ras proteins are proto-oncogenes that function as molecular switches linking extracellular stimuli with an overlapping but distinctive range of biological outcomes. Although modulatable interactions between the membrane and the Ras C-terminal hypervariable region (HVR) harbouring the membrane anchor motifs enable signalling specificity to be determined by their location, it is becoming clear that the spatial orientation of different Ras proteins is also crucial for their functions. To reveal the orientation of the G-domain at membranes, we conducted an extensive study on different Ras isoforms anchored to model raft membranes. The results show that the G-domain mediates the Ras–membrane interaction by inducing different sets of preferred orientations in the active and inactive states with largely parallel orientation relative to the membrane of most of the helices. The distinct locations of the different isoforms, exposing them to different effectors and regulators, coupled with different G-domain-membrane orientation, suggests synergy between this type of recognition motif and the specificity conferred by the HVR, thereby validating the concept of isoform specificity in Ras.

Keywords Membrane–protein interaction · Signalling · Ras · Model biomembranes

Abbreviations

aa	Amino acid
AFM	Atomic-force microscopy
ATR-FTIR	Attenuated total-reflection Fourier-transform infrared
DMPC	1,2-Dimyristoyl-*sn*-glycero-3-phosphocholine
DOPC	1,2-Dioleoyl-*sn*-glycero-3-phosphocholine
DOPG	1,2-Dioleoyl-*sn*-glycero-3-phospho-(1′-*rac*-glycerol)
DPPC	1,2-Dipalmitoyl-*sn*-glycero-3-phosphocholine
DPPG	1,2-Dipalmitoyl-*sn*-glycero-3-phospho-(1′-*rac*-glycerol)
HVR	Hypervariable region
IRRAS	Infrared reflection absorption spectroscopy
l_d	Liquid-disordered
l_o	Liquid-ordered
MD	Molecular dynamics
PM	Plasma membrane

Introduction

The peripheral membrane proteins of the proto-oncogenic Ras family connect cell-surface receptors with intracellular signalling cascades. Ras GTPases thus function as binary switches and, in their active GTP-bound state, regulate cell

Special Issue: Scattering techniques in biology—marking the contributions to the field of Peter Laggner, on the occasion of his 68th birthday.

S. Kapoor · K. Weise · M. Erlkamp · R. Winter (✉)
Physical Chemistry I, Biophysical Chemistry, Faculty of Chemistry, TU Dortmund University, Otto-Hahn-Str. 6, 44227 Dortmund, Germany
e-mail: roland.winter@tu-dortmund.de
URL: http://www.chemie.uni-dortmund.de/winter

G. Triola · H. Waldmann
Chemical Biology, Max Planck Institute of Molecular Physiology, Otto-Hahn-Str. 11, 44227 Dortmund, Germany

G. Triola · H. Waldmann
Faculty of Chemistry, TU Dortmund University, Otto-Hahn-Str. 6, 44227 Dortmund, Germany

proliferation, differentiation, and development, with Ras signalling being terminated by hydrolysis to Ras-GDP (Karnoub and Weinberg 2008; Wittinghofer and Pai 1991; Wittinghofer and Waldmann 2000). Two of the most abundant isoforms encoded by Ras genes are N-Ras and K-Ras, which are involved in tumourigenesis and developmental disorders (Bos 1989; Karnoub and Weinberg 2008; Schubbert et al. 2007; Waldmann and Rabes 1996; Wittinghofer and Waldmann 2000). Whereas the catalytic G-domain is highly conserved among Ras isoforms, the C-terminal hypervariable region (HVR) of Ras isoforms shares only 15 % sequence similarity. This HVR consists of an unstructured linker region and a Ras isoform-specific membrane anchor region that bears a farnesyl group at the terminal carboxymethylated cysteine residue in both N-Ras and K-Ras (Fig. 1). In contrast with N-Ras, which has a palmitoyl moiety at Cys^{181} as a second lipid anchor, the 4B splice variant of K-Ras (K-Ras4B) has a polybasic stretch of lysine residues as the second membrane-targeting signal that precedes the farnesylated cysteine (Wittinghofer and Waldmann 2000; Hancock et al. 1990; Hancock and Parton 2005). These post-translational modifications of Ras have been shown to be essential for correct functioning and location of Ras at the cytosolic leaflet of cellular membranes (Willumsen et al. 1984; Hancock and Parton 2005; Hancock et al. 1991).

In recent work by our group, a molecular mechanism for isoform-specific Ras signalling from separate membrane microdomains was postulated on the basis of the lateral organization of Ras proteins in heterogeneous model biomembranes (Weise et al. 2011). The results were obtained by performing time-lapse tapping-mode atomic-force microscopy (AFM) and confocal fluorescence microscopy experiments on the membrane partitioning of fully functional, lipidated N-Ras and K-Ras4B proteins, which were either GDP or GTP-loaded (GppNHp-bound state as a non-hydrolysable GTP analogue). Both N-Ras and K-Ras4B were shown to partition nearly exclusively into the liquid-disordered (l_d) phase of phase-separated membranes, irrespective of nucleotide loading and membrane composition. However, the Ras isoforms differ in their spatial distribution in heterogeneous membranes. Whereas time-dependent diffusion and subsequent clustering in the liquid-ordered/liquid-disordered (l_o/l_d) phase-boundary region of phase-separated membranes was observed for N-Ras (Weise et al. 2009; Vogel et al. 2009), formation of new protein-enriched domains inside a fluid environment was detected for K-Ras4B (Weise et al. 2011). Thus, Ras isoform-specific

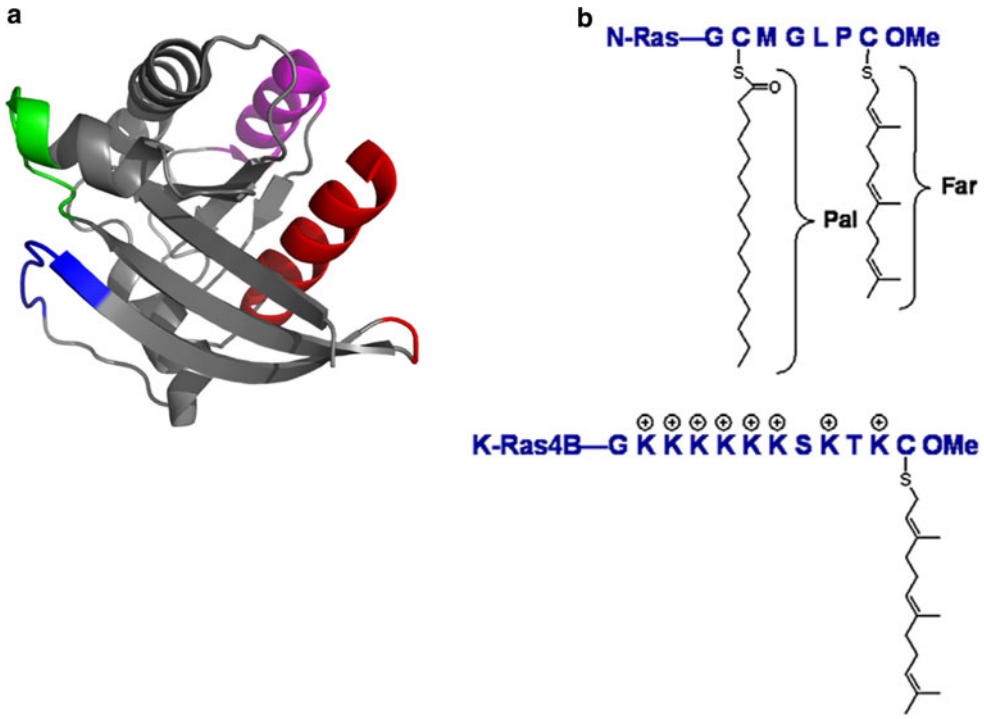

Fig. 1 Schematic representation of the semisynthetic Ras proteins used in this study. **a** Structure of the highly conserved G-domain of Ras, which has been adopted from the PDB (3GFT) to highlight the switch I region (aa 32–38; *blue*), switch II region (aa 59–67; *green*), switch III region, comprising the helix α5 (aa 151–167; *red*) and the β2–β3-loop (aa 47–49; *red*), and the helix α4 (aa 126–138; *magenta*). The image was generated by use of PyMOL. **b** Membrane anchors of N-Ras and K-Ras proteins (Brunsveld et al. 2009). The membrane anchor of all Ras isoforms is composed of a common C-terminal farnesylated (Far) and carboxymethylated cysteine residue. Whereas K-Ras4B contains a polybasic stretch of six contiguous lysine residues in a total of eight as a second membrane targeting signal, N-Ras bears a palmitoyl chain (replaced by a non-hydrolysable hexadecyl (HD) group as palmitoyl analogue in our study)

membrane microdomain formation or nanoclustering is caused by two different determinants: minimization of the line energy by expulsion of N-Ras proteins to the interfacial region of heterogeneous membranes and electrostatic interactions between the positively charged lysines of K-Ras4B and the phospholipid headgroups, i.e., an effective lipid sorting mechanism. Moreover, nanoclustering of Ras has also been shown to be critical for signal transmission across the plasma membrane (Tian et al. 2007).

Although Ras isoform-specific membrane partitioning caused by the C-terminal HVR of Ras has been reported, the question which arises is whether there is also a structural component of the catalytic G-domain that contributes to Ras isoform-specific signal outputs after interaction with overlapping downstream effectors at the plasma membrane. The first data on structural and dynamical aspects of full-length Ras–membrane interactions were derived from molecular dynamics simulations and verified by Förster resonance energy transfer (FRET) and fluorescence lifetime imaging microscopy (FLIM) combined with an ERK activation and PC12 differentiation cell assay (Gorfe et al. 2007a, b; Abankwa et al. 2008b). Altogether, the results led to the identification of a novel conformational switch III region that is involved in the reorientation of the H-Ras catalytic domain at lipid membranes and comprises the β2–β3-loop and helix α5 (Abankwa et al. 2008b) (Fig. 1). Furthermore, a so-called "balance model" was proposed that illustrates the modulation of the Ras G-domain plasma membrane orientation through the α4-helix of the G-domain and the HVR, switching H-Ras in a GTP/GDP-dependent manner between two modes of membrane binding (Gorfe et al. 2007b; Abankwa et al. 2008a, b). Because sequence alignment of Ras isoforms revealed high divergence for both helix α4 and the HVR (Abankwa et al. 2008b), these two structural elements could cause Ras isoform diversity by inducing distinct G-domain orientations for the active Ras isoforms. In support of this hypothesis, recent MD simulations of K-Ras complexed with a DMPC lipid bilayer in combination with biochemical experiments on a K-Ras4B-like chimera indicated an inverted interaction profile for the G-domain of membrane-bound K-Ras compared with H-Ras (Abankwa et al. 2010). However, biophysical experiments that directly detect conformational and orientational changes in the G-domain of fully lipidated, wild-type Ras isoforms upon membrane binding—and especially in the presence of heterogeneous membranes for K-Ras4B—are largely missing. Some initial work by our group on these issues, using Fourier-transform infrared (FTIR) spectroscopy, revealed no significant changes in secondary structure upon interaction of N-Ras and K-Ras4B with heterogeneous model membranes (Weise et al. 2011; Kapoor et al. 2012). However, in combination with infrared reflection absorption spectroscopy (IRRAS) data, preferred structural reorientations of the G-domain could be revealed for both proteins during Ras–membrane interaction, and the orientational flexibility was shown to be dependent on nucleotide loading (Weise et al. 2011; Meister et al. 2006; Kapoor et al. 2012). In particular, essentially parallel orientation relative to the membrane of most of the helices in the G-domain of N-Ras was observed by polarized ATR-FTIR spectroscopy; this was confirmed and further itemized by simulation of IRRA spectra (Kapoor et al. 2012). To broaden these studies, this work focusses on the orientation of K-Ras4B at negatively charged, heterogeneous membranes. To this end, polarized ATR-FTIR spectroscopic experiments were conducted to determine relative changes in the orientation of the protein in its different nucleotide-bound states in the presence of these heterogeneous lipid bilayers. Furthermore, complementary IRRAS experiments were conducted in the presence of analogous heterogeneous lipid monolayers on different K-Ras4B proteins, yielding information on the membrane insertion process and associated orientational changes. Finally, we compare these results with those recently obtained for N-Ras under similar conditions and introduce a hypothesis for conformational selection of Ras proteins at membranes.

Materials and methods

Materials

The phospholipids 1,2-dioleoyl-*sn*-glycero-3-phosphocholine (DOPC), 1,2-dioleoyl-*sn*-glycero-3-phospho-(1′-*rac*-glycerol) sodium salt (DOPG), 1,2-dipalmitoyl-*sn*-glycero-3-phospho-(1′-*rac*-glycerol) sodium salt (DPPG), and 1,2-dipalmitoyl-*sn*-glycero-3-phosphocholine (DPPC) were purchased from Avanti Polar Lipids (Alabaster, AL, USA). Cholesterol (Chol) was purchased from Sigma–Aldrich (Deisenhofen, Germany). All other reagents and solvents were obtained from Sigma–Aldrich and Merck (Darmstadt, Germany). The lipids were used without further purification.

Protein synthesis

The synthesis of N-Ras HD/Far and K-Ras4B Far has been described in detail elsewhere (Nagele et al. 1998; Kuhn et al. 2001; Chen et al. 2010; Brunsveld et al. 2006). Briefly, double lipidated N-Ras protein was synthesized by maleimide ligation of the N-Ras peptide carrying an N-terminal maleimide group and the bacterially expressed N-Ras protein core with only one surface accessible cysteine at the C-terminus (Weise et al. 2009). In contrast with the resulting non-natural thioether bond of N-Ras, K-Ras4B has a native amide bond after ligation.

S-Farnesylated K-Ras4B was synthesized by expressed protein ligation (EPL) which involved ligation of the additional N-terminal cysteine of the K-Ras4B peptide with the truncated K-Ras4B protein core thioester (Chen et al. 2010). For the active form of both Ras proteins, a non-hydrolysable analogue of GTP, GppNHp, was used. Details of the nucleotide exchange can be found elsewhere (Weise et al. 2009, 2011).

Polarized attenuated total-reflection Fourier-transform infrared (ATR-FTIR) spectroscopy

Stock solutions (10 mg mL^{-1}) of the lipids DOPC, DOPG, DPPC, and Chol in chloroform (Merck) and DPPG in 3:1 chloroform–methanol (Merck) were prepared and mixed to obtain the desired composition of the neutral lipid raft mixture (DOPC–DPPC–Chol 50:25:50 (molar ratio) for measurements with N-Ras) and anionic lipid raft mixture (DOPC–DOPG–DPPC–DPPG–Chol 20:5:45:5:25 (molar ratio) for measurements with K-Ras4B) (Zhai et al. 2011; Kapoor et al. 2011). Most of the chloroform was evaporated with a nitrogen stream; all remaining solvent was subsequently removed by drying under vacuum overnight. The dry lipid mixture was hydrated with 20 mM Tris (Merck) and 5 mM (for the neutral raft mixture) or 7 mM (for the anionic raft mixture) $MgCl_2$ (Merck) D_2O buffer, pD 7.4. The hydrated lipid mixture was then vortex mixed, kept in a water bath at 65 °C for 15 min, and sonicated for 10 min. After five freeze–thaw–vortex cycles and brief sonication, large multilamellar vesicles were formed and transformed to large unilamellar vesicles of homogeneous size by use of an extruder (Avanti Polar Lipids) with polycarbonate membranes of 100 nm pore size at 65 °C.

Polarized ATR-FTIR spectra were recorded by use of a Nicolet 6700 infrared spectrometer attached to a wire grid infrared automated ZnSe polarizer (Pike Technologies). Spectra were combinations of 256 scans taken with a spectral resolution of 2 cm^{-1} at both 0° and 90° polarization. The ATR out-of-compartment accessory consists of a liquid jacketed Piketech ATR flow-through cell with a trapezoidal Ge-crystal (Resultec Analytical Equipment, Germany; 80 × 10 × 4 mm^3; angle of incidence 45°). The ATR flow-cell was maintained at 25 °C and a buffer spectrum at both polarizations was taken before the measurement. A freshly prepared solution of large unilamellar vesicles of the required composition was injected into the ATR flow-cell, which was heated to 60 °C. Direct spreading of the sonicated vesicles produced lipid bilayers, especially if the buffer contained ≥1 mM divalent cations, for example the $MgCl_2$ used in this study (Papahadjopoulos et al. 1976). After adsorption overnight and cooling to 25 °C, the membrane was washed with buffer for 2 h to remove any loosely bound lipid vesicles. The protein solutions ($c = 4$ μM) were then injected into the ATR cell and polarized spectra were taken every 10 min up to 33 h and obtained after background subtraction, one level of zero filling, and Blackman–Harris three-term apodisation. The dichroic spectra (details of the calculation are given in the next section) have been smoothened by use of a nine-point-Savitzky–Golay function, where needed.

Orientation of Ras at membranes

In polarized ATR-FTIR spectroscopy, all the orientation information is contained within the dichroic ratio R^{ATR} as defined by Eq. (1):

$$R^{\mathrm{ATR}} = \frac{A^{\mathrm{II}}}{A^{\perp}}, \tag{1}$$

where A^{II} and $A^{\perp}$ refer to the integrated absorbance of a band measured with parallel and perpendicular polarized light, respectively. This dichroic ratio is related to the orientational order parameter S by Eq. (2):

$$R^{\mathrm{ATR}} = \frac{E_x^2}{E_y^2} + \frac{E_z^2}{E_y^2}\left(1 + \frac{3S}{1-S}\right), \tag{2}$$

where E_x^2, E_y^2, and E_z^2 are the time-averaged square electric field amplitudes of the evanescent wave in the film at the Ge/film interface. Equation (2) assumes uniaxial symmetry. Within the thin-film approximation (film much thinner than the penetration depth of the evanescent wave), the electric field values are described by Eqs. (3)–(5), whereas Eqs. (6)–(8) correspond to the field values for the thick-film model (film much thicker than the penetration depth of the evanescent wave) (Harrick 1967).

$$E_x = \frac{2\cos\theta\sqrt{\sin^2\theta - n_{31}^2}}{\sqrt{1-n_{31}^2}\cdot\sqrt{(1+n_{31}^2)\sin^2\theta - n_{31}^2}} \tag{3}$$

$$E_z = \frac{2\cdot n_{32}^2\cos\theta\sin\theta}{\sqrt{1-n_{31}^2}\cdot\sqrt{(1+n_{31}^2)\sin^2\theta - n_{31}^2}} \tag{4}$$

$$E_y = \frac{2\cos\theta}{\sqrt{1-n_{31}^2}} \tag{5}$$

$$E_x = \frac{2\cos\theta\sqrt{\sin^2\theta - n_{21}^2}}{\sqrt{1-n_{21}^2}\cdot\sqrt{(1+n_{21}^2)\sin^2\theta - n_{21}^2}} \tag{6}$$

$$E_z = \frac{2\cos\theta\sin\theta}{\sqrt{1-n_{21}^2}\cdot\sqrt{(1+n_{21}^2)\sin^2\theta - n_{21}^2}} \tag{7}$$

$$E_y = \frac{2\cos\theta}{\sqrt{1-n_{21}^2}} \tag{8}$$

where $n_{31} = n_3/n_1$, $n_{21} = n_2/n_1$, $n_{32} = n_3/n_2$ and θ is the angle of incidence of the IR beam at the solid–lipid interface. In this study, the refractive index values used were $n_1 = 4.0$ (Ge), $n_2 = 1.43$–1.45 (lipids and proteins), and $n_3 = 1.32$ (D_2O), with $\theta = 45°$.

In addition to the quantitative order parameter S, qualitative information on the orientation of molecular constituents can be obtained from the dichroic spectra, which are, in turn, obtained by subtracting the perpendicular polarized spectra ($A_\perp$) from the parallel polarized spectra (A_{II}) by use of Eq. (9). The scaling coefficient used to compute the dichroic spectra is the dichroic ratio for an isotropic sample, R_{iso}^{ATR}, which is given by Eq. (10). It is the dichroic ratio of a transition dipole that is either spatially disordered or oriented at the magic angle and takes into account different relative power of the evanescent field for each polarization and the film thickness.

$$\Delta A = A_{II} - R_{iso}^{ATR} \cdot A_\perp \tag{9}$$

$$R_{iso}^{ATR} = \frac{E_x^2 + E_z^2}{E_y^2} \tag{10}$$

Using the values of refractive indices and θ as mentioned above, the computed value of R_{iso}^{ATR} ranges between 1.712 and 2.0 for thin and thick films, respectively, indicating the need to take the film thickness into account. Recent studies revealed that measured dichroic ratios including R_{iso}^{ATR} depend on the amount of material used to make each film and hence on film thickness (Bechinger et al. 1999), calling into question the appropriateness of the thick and thin film hypothesis for each sample preparation. Furthermore, only the electric field amplitude along the z-axis (E_z), and thus, R_{iso}^{ATR} significantly depends on n_2, n_3, and the film thickness d. In this study, application of the thin-film approximation results in unreliable dichroisms for the lipid bands, indicative of the presence of intermediate or thick films.

Advances in this method and the availability of two, three, and four-phase approximations have undoubtedly contributed to resolving this uncertainty, which is neither minor nor subtle, regarding use of a valid model and its associated R_{iso}^{ATR} value for calculating the dichroic spectra (Goormaghtigh et al. 1999; Axelsen and Citra 1996; Ausili et al. 2011). A well established approximation of R_{iso}^{ATR} can be obtained experimentally by using the lipid ester ν(C=O) band (1,762–1,700 cm^{-1}). The dichroic spectra are computed by zeroing the area of the lipid ester band near 1,738 cm^{-1} (Bechinger et al. 1999). The rationale behind this originates from the fact that the lipid ester ν(C=O) band is thought to have a transition oriented close to the magic angle (54.7°), as supported by ^{13}C and ^{1}H NMR spectroscopic experiments (Wittebort et al. 1981; Smith et al. 1992). Furthermore, fast conformational exchange coupled with axial diffusion and molecular motion are in agreement with an apparently isotropic signal of the ester C=O stretch vibration (Lewis and McElhaney 1992). This method has been proved to be suitable for the spectral analysis performed in this study by verifying that the value of R_{iso}^{ATR} calculated in this way is consistent with the dichroism of other lipid bands, i.e., confirming the perpendicular orientation of the lipid acyl chains relative to the germanium surface by dichroic ratios lower and higher than R_{iso}^{ATR} for $\nu_s(CH_2)$ and $\nu_{as}(CH_3)$, respectively. The advantage of using this method is that it not only enables changes in the relative power of evanescent fields to be taken into account but also the "real" film thickness. Although it must be noted that the lipid ester band provides just an approximation of R_{iso}^{ATR}, it has been shown to be accurate enough for deriving the orientation of lipid and protein in films of different thickness (Goormaghtigh et al. 1999) and hence was used in this study.

Infrared reflection absorption spectroscopy (IRRAS)

The IRRAS equipment has been described in detail elsewhere (Meister et al. 2006; Kapoor et al. 2012). Briefly, infrared spectra were recorded by use of a Vertex 70 FT-IR spectrometer (Bruker, Germany) equipped with a variable-angle reflectance accessory, the A511 (Bruker). The accessory is a self-contained computer-controlled unit coupled to a custom-designed Langmuir trough (Riegler, Germany) with a Wilhelmy plate as pressure sensor. Two Teflon troughs of different sizes are linked by two pieces of small-bore tubing to ensure equal heights of the air–D_2O interface in both troughs. The temperature of the subphase was maintained at 20 ± 0.5 °C and measurements were performed in the small (reference) trough at constant area and with the large trough filled with buffer solution, only. The IR beam is focussed by several mirrors on to the subphase, and different angles of incidence can be used. A wire grid polarizer is placed into the optical path just before the point at which the beam impinges on the aqueous phase. The reflected light is collected at the same angle as the angle of incidence, and is directed on to a nitrogen cooled MCT detector. The trough system was positioned on a movable platform to enable shuttling between sample and reference troughs, thereby reducing the spectral interference because of absorption by water vapour in the light beam. The entire experimental setup was enclosed and purged to keep the relative humidity both low and constant.

IRRAS sample preparation and spectra acquisition

A D_2O based subphase consisting of 100 mM NaCl, pD 7.4 was used for all experiments. DOPC–DPPC–Chol (25:50:25) and DOPC–DOPG–DPPC–DPPG–Chol (20:5:45:5:25) monolayers were formed by directly spreading the lipid solution (1 mM) in a mixture of chloroform and methanol on the subphase. Protein adsorption measurements were performed by injection of a concentrated protein solution into the subphase beneath the monolayers (kept at 10 mN m^{-1} for N-Ras and 30 mN m^{-1} for K-Ras4B) to yield a concentration of 200 nM.

For each spectrum, 2,000 scans were acquired at $\sim$8 cm^{-1} resolution, co-added, apodised with a Blackman–Harris three-term function with a zero filling factor of 2 to produce spectra encoded at $\sim$4 cm^{-1} intervals. The IRRA spectra are depicted as plots of reflectance–absorbance (RA) versus wavenumber. RA is defined as $-\log(R/R_0)$ where R is the reflectivity of the film-covered trough and R_0 is the reflectivity of the buffer. After reaching a constant surface pressure (equilibrium state), measurements at different angles of incidence using parallel (p) and perpendicularly (s) polarized light were performed. Comparing the amide-I′ band taken with p-polarized light at different angles of incidence furnishes information on the orientation of the protein at the monolayer interface. The measured IRRA signal can be either positive or negative, depending on the angle of incidence, its proximity to the Brewster angle, and the orientation of the transition dipole moment of the probe relative to the interface. At a given angle of incidence above the Brewster angle, positive intensities imply a transition dipole oriented preferentially in the surface plane, and negative intensities reflect perpendicular orientation.

To demonstrate the stability and integrity of the pure lipid monolayer film, Fig. 2 shows the surface pressure profile and the IRRA spectra depicting the lipid bands (CH_2 asymmetric stretch at 2,923 cm^{-1} and symmetric stretch at 2,953 cm^{-1}) over a time period of 24 h. Both remained essentially constant over the entire time period of the experiment, implying long-term stability of the anionic lipid monolayer film. Similar behaviour was observed for the neutral raft lipid monolayer (IRRA spectra not shown).

Results

Interaction of Ras isoforms in different nucleotide states with heterogeneous lipid bilayers

Ras GTPases are plasma membrane (PM)-associated proteins, and the inherent properties of the PM in respect of lipid composition, charge, and phase behaviour are believed to be of crucial importance in the regulation of signalling processes (Simons and Toomre 2000). There is increasing evidence that the lateral organization of the PM, i.e., segregation into raft and non-raft microdomains, provides a unique environment for the signalling proteins to locally concentrate proteins and generate distinct signalling platforms (Tian et al. 2007; Simons and Toomre 2000). Keeping this in mind, we used lipid monolayers and bilayers of different composition and charge, including heterogeneous raft like structures (Evers et al. 2012), as model systems to study Ras–membrane interactions.

Polarized ATR-FTIR spectroscopy was used to examine relative changes in the orientation of the Ras isoforms in their different nucleotide-bound states upon insertion into heterogeneous raft bilayers. This is a well established technique for determining the secondary structure and orientation of proteins at solid or lipid interfaces (Marsh 1999; Goormaghtigh et al. 1999). Qualitative analysis of the membrane orientation of the Ras protein is easily performed by examining the dichroic spectrum, which, in turn, is obtained by use of Eq. (9). In the absence of any preferred orientation, a straight horizontal line is expected. An upward deviation indicates a transition dipole moment

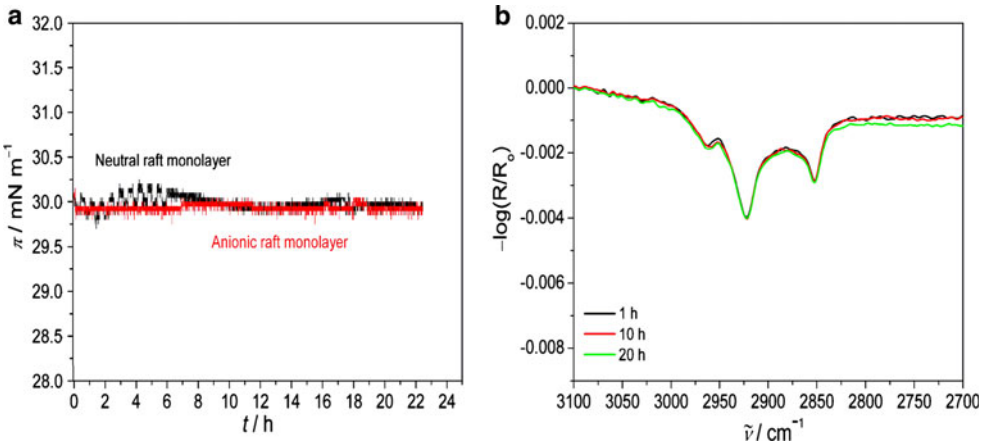

Fig. 2 **a** Surface pressure versus time course of anionic and neutral raft lipid monolayers composed of DOPC–DOPG–DPPC–DPPG–Chol (20:5:45:5:25, molar ratio) and DOPC–DPPC–Chol (25:50:25), respectively, kept at $\sim$30 mN m^{-1}. **b** IRRA spectra are shown for the lipid band region of the anionic raft monolayer over 20 h. All IRRA spectra were recorded with p-polarized light at a 35° angle of incidence and 25 °C

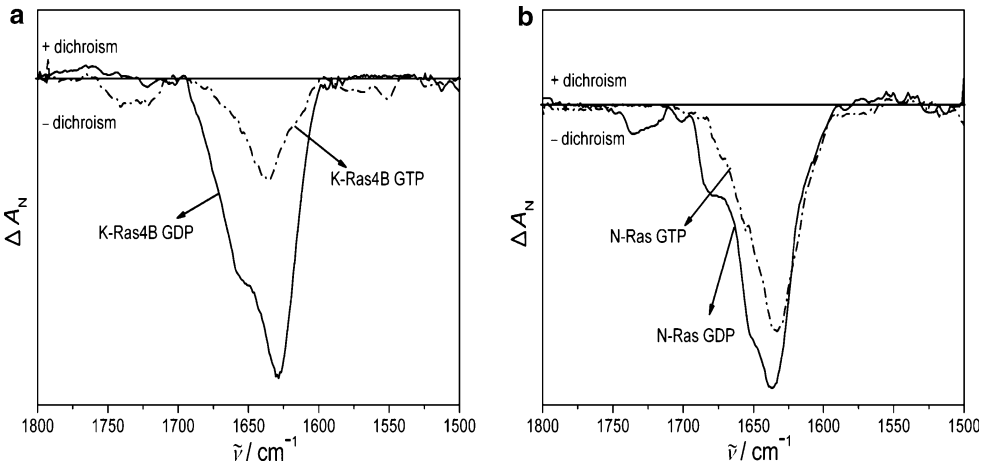

Fig. 3 ATR-FTIR dichroic spectra of **a** K-Ras4B GDP/GTP in the presence of anionic lipid raft bilayers composed of DOPC–DOPG–DPPC–DPPG–Chol (20:5:45:5:25, molar ratio) and **b** N-Ras GDP/GTP in the presence of neutral lipid raft bilayers composed of DOPC–DPPC–Chol (25:50:25, molar ratio) at 25 °C after equilibration (i.e., 20 h). ΔA_N is the absorbance normalized to the sum of the area under the amide-I′ band for both the parallel and perpendicular polarized spectra

approximately parallel to the membrane normal. Conversely, a downward deviation indicates preferred alignment of the dipole in the membrane plane.

Figure 3a shows the dichroic spectra for GDP and GTP-loaded K-Ras4B bound to an anionic lipid raft bilayer under equilibrium conditions. The observed changes in the magnitude of the dichroism imply that, on average, K-Ras4B GTP is more or less randomly orientated, as indicated by the low magnitude of dichroism, presumably because of many different orientations of the G-domain when bound to GTP. Conversely, K-Ras4B in the inactive form has strong negative dichroism implying preferred orientation at the membrane interface. Negative deviations in the helix region (1,648–1,665 cm^{-1}) of the amide-I′ band region indicate orientation of most of the helices in K-Ras4B essentially parallel to the lipid bilayer, because, for the α-helix, the stronger component of the amide-I transition dipole is along the helix long axis. Furthermore, differences in the wavenumber maxima of the amide-I′ bands suggest differences in the strength of interaction with the membrane, being stronger for K-Ras4B GDP (amide-I′ band maximum at ~1,629 cm^{-1}) than for K-Ras4B GTP (amide-I′ band maximum at ~1,635 cm^{-1}). These results are supported by recent results of Lukman et al. (2010), who used molecular dynamics (MD) simulations to show that the flexibility of the wild type K-Ras bound to GTP was greater than for other isoforms. To further show that orientation sensitivity is important to Ras proteins in general, the dichroic spectra of another Ras isoform, N-Ras HD/Far (both GDP and GTP-bound), in the presence of a lipid bilayer (Fig. 3b; reproduced and modified from Kapoor et al. 2012), was compared with that of K-Ras4B. From the negative deviations in the helix region (1,648–1,665 cm^{-1}) of the amide-I′ band it can be inferred that N-Ras in both nucleotide bound states has preferred orientations with most of the helices oriented essentially parallel to the membrane interface, with slightly stronger membrane interaction with N-Ras GTP (amide-I′ maximum at ~1,633.5 cm^{-1}) than with N-Ras GDP (amide-I' band maximum at ~1,637 cm^{-1}).

It should be noted that in Ras only three of five helices are essentially parallel to each other and the central β-sheet is twisted so that the different contributions of the transition dipoles arising from the respective secondary structure elements lead to some ambiguity in the calculation of orientational coordinates from ATR-FTIR data. What is clear, however, is that Ras isoforms adopt conformations with most of the helices in the parallel orientation relative to the membrane interface, as is evident from the strong negative amide-I′ band in the dichroic spectra. Similar qualitative results were obtained for the membrane orientation of Ras when using R_{iso}^{ATR} values (cf. "Materials and methods") calculated by use of the thin and thick-film approximations, with different magnitudes of negative dichroism, however.

Interaction of Ras isoforms in different nucleotide states with heterogeneous lipid monolayers

The membrane anchor of Ras proteins (C-16/C-14) is expected to insert into and span only one leaflet of a lipid bilayer (that is, the inner leaflet of the PM). Because lipid raft-like ordered domains were recently also detected in neutral and anionic lipid monolayers of the corresponding lipid compositions (Evers et al. 2012), studies on lipid monolayers can complement lipid bilayer work. To study the membrane insertion of Ras proteins upon membrane interaction by use of lipid monolayers at the water/air interface, infrared reflection absorption (IRRA) spectroscopy was used; this enables monitoring of the combined effects of orientational and structural changes of proteins that are inserted into lipid monolayers, including changes in the strength of the interaction, by measuring the surface pressure profile simultaneously with IRRA spectra (Mendelsohn et al. 2010). Because no major secondary structural changes occur in Ras isoforms upon membrane insertion

(both for monolayers and bilayers, in agreement with previous reports (Weise et al. 2011; Meister et al. 2006; Kapoor et al. 2012; Güldenhaupt et al. 2008)) this enables us to delineate the spectral shifts, intensity, and shape changes of the amide-I′ band on account of the protein orientational changes and the strength of interaction with the membrane. The α-helices and β-sheet substructures have different orientations relative to the membrane interface in the different overall orientations of Ras, leading to different contributions of the individual secondary structure elements of the protein to the observed amide-I′ band contour. By simultaneously recording IRRA spectra and surface pressure/time (π/t) isotherms, the interaction of K-Ras4B and N-Ras HD/Far (both GDP and GTP-bound) with lipid monolayers composed of the anionic and neutral raft mixture, respectively, was studied and the associated changes examined. As a control, the long-term stability of the pure lipid monolayer on the aqueous subphase was ensured by collecting a π/t isotherm over 22 h and observing an almost constant surface pressure profile with no significant changes in the lipid bands over the whole time frame (Fig. 2). The long-term stability of the Ras protein was also checked by analysis of the secondary structure of membrane-bound Ras by FTIR spectroscopy (Fig. 4).

Injection of K-Ras4B proteins beneath the lipid monolayer was accomplished at a surface pressure of approximately 28–30 mN m^{-1}, which reflects the physiological lipid density generally found in lipid membranes. Figure 5a shows the π/t-profile, which is indicative of effective insertion of the farnesyl anchor of K-Ras4B in both nucleotide-bound states into the lipid monolayer, resulting in a significant increase ($\Delta\pi \approx 4.5$–6 mN m^{-1}) in surface pressure with progressing membrane insertion. This is reemphasized by the fact that no insertion (only slight perturbation of the baseline) was observed for unlipidated K-Ras4B. A slightly larger initial slope and higher plateau for K-Ras4B GTP compared with K-Ras4B GDP might imply slightly faster and stronger incorporation of the active form.

The IRRA spectra of the amide-I′ region of K-Ras4B GDP (Fig. 5b) reveal a stable band maximum between 1,639 and 1,641 cm^{-1}, arguing for a relatively fixed or less flexible orientation of the protein in this state. A small shift in wavenumber of the band maximum between 1,636 and 1,643 cm^{-1} is seen for the active protein within the experimental time frame (Fig. 5c), suggesting greater orientational flexibility of the protein at the lipid interface. Please note that the IRRAS measurements were carried out under diffusion control, i.e., on a drastically expanded time scale compared with the physiologically relevant case. Because the proteins take longer to insert in the monolayers (on the hours time scale in the experimental arrangement used), the concomitant changes in the conformations or orientations could be spread out in time, which enabled collection of IRRA spectra over a long time period. The spectral changes observed match reasonably well with the time-dependent AFM data, indicating that the orientational changes observed might very well be attributed to the conformational constraints imposed by the clustering of the Ras isoforms in the lipid bilayer plane. Hence, the spectral changes observed might be linked to the orientational substates the proteins are likely to adopt in the membrane-bound state. The absorption intensity is almost a factor of three lower for the unlipidated K-Ras4B, because of adsorption at, but no insertion into, the lipid monolayer (Fig. 5d), and the amide-I′ band for this unlipidated, GDP-loaded K-Ras4B suggests reorientational flexibility

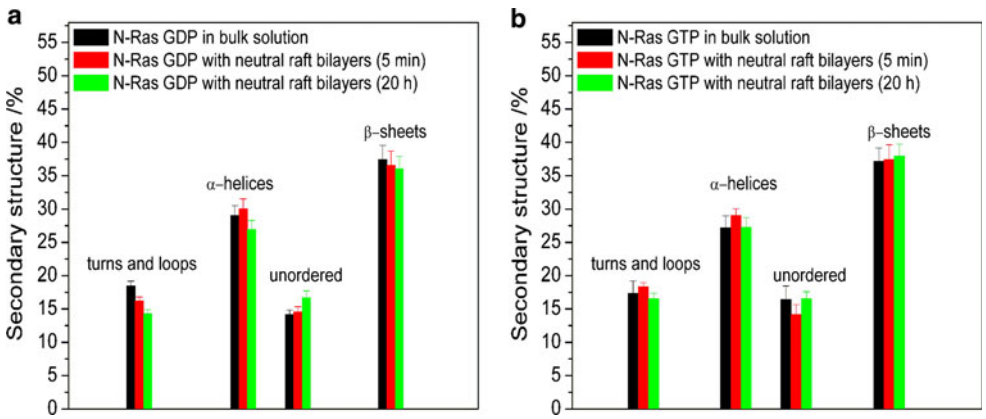

Fig. 4 Structural evaluation of the GDP and GTP-loaded N-Ras in the bulk and bound to neutral raft bilayers composed of DOPC–DPPC–Chol (25:50:25). Peak fitting of the normalized FTIR spectra yields the secondary structural elements of N-Ras HD/Far GDP (**a**) and N-Ras HD/Far GTP (**b**) in the bulk solution and in the membrane-bound form at selective time points at 25 °C. Within the experimental error of a few percent, no significant changes in secondary structure occur upon membrane interaction with time. The same behaviour has been observed for K-Ras4B proteins (Weise et al. 2011)

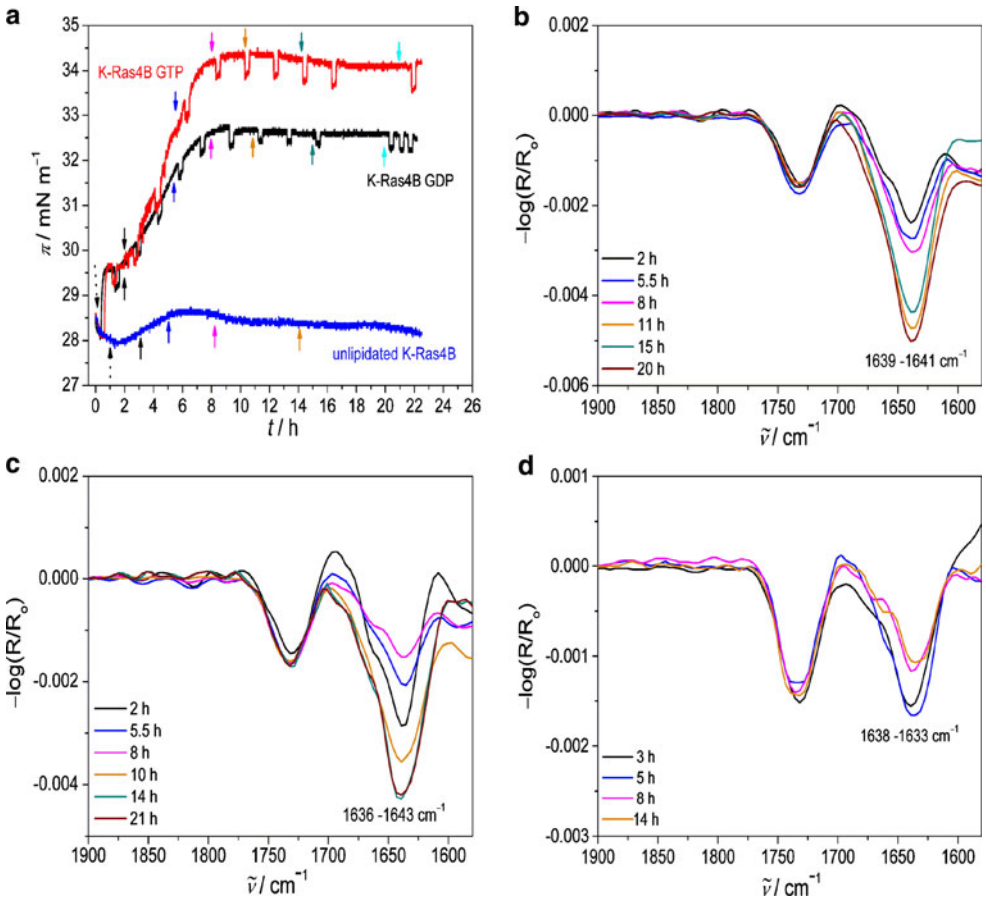

Fig. 5 **a** Surface pressure versus time course after injection of K-Ras4B GDP/GTP or unlipidated K-Ras4B (200 nM each) beneath an anionic raft lipid monolayer composed of DOPC–DOPG–DPPC–DPPG–Chol (20:5:45:5:25, molar ratio), initially kept at $\sim$30 mN m^{-1}. IRRA spectra are shown for the amide-I′ region of **b** K-Ras4B GDP, **c** K-Ras4B GTP, and **d** unlipidated K-Ras4B at the respective positions of the surface pressure versus time curve as indicated by *arrows* (**a**). All IRRA spectra were recorded with p-polarized light at a 35° angle of incidence and 25 °C

comparable with that of the G-domain of active K-Ras4B at anionic raft membranes, as indicated by the shift of the band maximum between 1,633 and 1,638 cm^{-1}.

Comparison with a similar study on N-Ras proteins (Fig. 6) reveals differences in the mode of interaction with the lipid monolayer. The IRRA spectra for the amide-I′ region of N-Ras HD/Far GDP/GTP reveal a shift in wavenumber between approximately 1,638/39 and 1,632 cm^{-1} for N-Ras GDP and 1,626 cm^{-1} for N-Ras GTP, within the analyzed time period, suggesting some reorientation of both proteins upon membrane insertion. The temporal evolution of the amide-I′ band maxima for K-Ras4B (Fig. 5b, c) and N-Ras (Fig. 6a, b) suggests different orientational flexibility of the Ras isoforms at the membrane interface. For N-Ras, the corresponding π/t isotherms (Fig. 6c) are indicative of effective insertion of the two lipid anchors of N-Ras in both nucleotide-bound states into the lipid monolayer, as is evident from the marked increase in surface pressure ($\Delta\pi \approx$ 15.5–17 mN m^{-1}). The time evolution of the surface pressure shows somewhat faster adsorption of N-Ras GTP, implying slightly higher membrane affinity for the active N-Ras. This suggests that the membrane affinity is modulated by the bound nucleotide state. A lower initial surface pressure of the lipid monolayer (10 mN m^{-1}) was chosen for the N-Ras measurements, because N-Ras proteins with two lipid anchors (HD and Far) were unable to produce a significant increase in surface pressure after insertion, when injected beneath a lipid monolayer kept at 30 mN m^{-1}, as reported elsewhere (Meister et al. 2006). This does not imply that N-Ras HD/Far is incapable of inserting into the lipid monolayer at 30 mN m^{-1}, but rather that N-Ras HD/Far insertion produces an increase in surface pressure that is too small to be detected by the instrument. To test this hypothesis, experiments were also conducted with different N-Ras constructs with different numbers of lipid anchor motifs in the HVR region, under similar experimental conditions but with injection beneath a lipid monolayer kept at 30 mN m^{-1} (Fig. 6d). N-Ras bearing one Far group can easily insert into the membrane, with a significant increase in surface pressure; no such effect was observed for unlipidated N-Ras or N-Ras bearing two lipid anchors. Small changes seen in the surface pressure profile for the unlipidated Ras proteins can probably be attributed to perturbation of the lipid monolayer upon adsorption of the proteins at the lipid interface, without stable insertion, however. This effect observed for unlipidated N-Ras and K-Ras4B is likely to arise from insertion of hydrophobic side chains of the

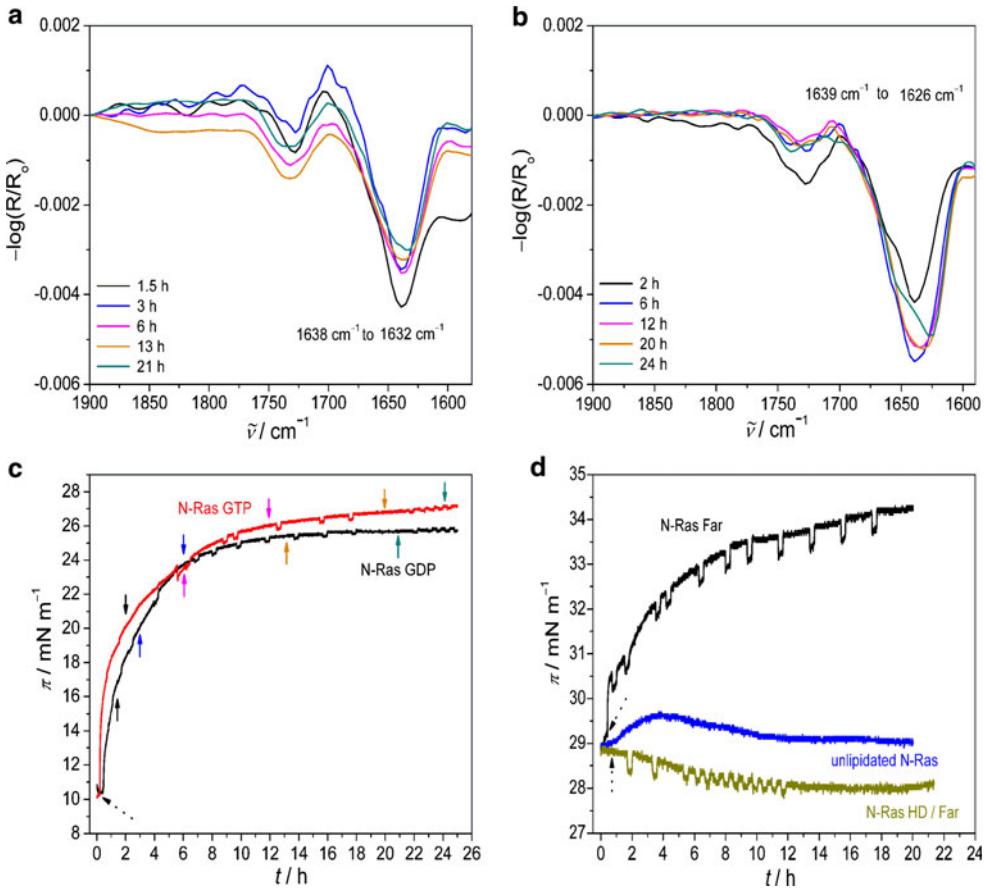

Fig. 6 IRRA spectra of the amide-I′ region of **a** N-Ras GDP and **b** N-Ras GTP at the respective positions (indicated by *arrows*) of the surface pressure versus time curve (**c**).The surface pressure versus time course is given for neutral raft lipid monolayers composed of DOPC–DPPC–Chol (25:50:25, molar ratio) initially kept at **c** ~10 mN m^{-1} after injection of N-Ras GDP/GTP (200 nM each) and **d** ~30 mN m^{-1} after injection of N-Ras Far, N-Ras HD/Far, and unlipidated N-Ras (200 nM each). All IRRA spectra were recorded with p-polarized light at a 35° angle of incidence and 25 °C

protein into the hydrophobic region of the membrane. This would be in agreement with X-ray diffraction (GIXD) and specular reflectivity (XR) studies on the adsorption of lipidated N-Ras protein on lipid monolayers, in showing that insertion of hydrophobic side chains of the Ras protein is feasible and required for stabilizing the protein at the interface (Bringezu et al. 2007). Furthermore, similar studies on lipid bilayers also revealed that the backbone of the C-terminus of the lipid modified Ras is preferentially localized at the lipid/water interface, where the lipid modification and the hydrophobic side chain of the lipidated Ras peptide are able to deeply insert into the membrane (Huster et al. 2001).

Discussion and conclusions

Ras signalling is strongly affected by binding to specific effectors, many of which are also membrane-associated. Thus, any change in the conformation, orientation, and location of membrane-bound Ras proteins is reflected in modified binding to different effectors/regulators and, consequently, cell signalling. In recent years, much research has revealed that Ras isoforms generate distinct signal outputs, despite using a shared set of effectors and regulators, and finally activate common signalling pathways to different extents (Yan et al. 1998). Thus, one of the questions most investigated in Ras signalling is: what are the determinants of these specific interactions?

One of the structural components of Ras that are expected to contribute to the observed biological differences in the isoforms is the C-terminal HVR, which is post-translationally lipidated and anchors the G-domain to the membrane. Our previous studies have revealed that this region is associated with isoform-specific location and lateral segregation of Ras proteins in membranes, forming specific nanoclusters in distinct parts of heterogeneous model biomembranes (Weise et al. 2009, 2011; Vogel et al. 2009). It is hypothesized these distinct membrane microenvironments affect Ras signalling outputs, thus generating high-fidelity signalling platforms, in accord with many in-vivo studies (Hancock 2003; Walsh and Bar-Sagi 2001; Prior et al. 2003). In addition to the HVR, members of the Ras superfamily of small GTP-binding proteins harbour a structurally and mechanistically preserved GTP-binding core, the G-domain. Recently, mathematical modelling and FRET/FLIM microscopy were used to reveal the dynamic interplay between the orientations of the G-domain and variable signalling output, i.e., MAPK activation (Gorfe et al. 2007a, b). In these in-vivo studies, the observed

differences in phenotypic behaviour of RasG12V compared with mutants (alanine substitutions in α-4 and HVR) were correlated with different signalling activity via plausible changes in G-domain orientation. Possible conformational changes induced by the mutations themselves might render the analysis quite cumbersome, however, coupled with potential signalling artefacts associated with tagging and over-expression of proteins.

To investigate the orientation of the G-domain at membranes, we conducted an extensive biophysical study on different Ras isoforms anchored to model raft lipid monolayers and bilayers. Furthermore, the effect of different nucleotide states of the same Ras isoform was investigated. Besides demonstration of the HVR and nucleotide-modulated binding of Ras isoforms to lipid bilayers and monolayers, determination of the orientation of the proteins was attempted by performing simulations of the amide-I contour at different angles of incidence with polarized light. To this end, the experimental IRRA spectra were acquired at different angles of incidence with p-polarized light at a time point at which an equilibrium state was reached. For all Ras isoforms, a switch in the sign of the IRRA amide-I′ signal at an angle of incidence above the Brewster angle was obtained (with different intensities, however), which is indicative of, on average, parallel alignment of most of the helices relative to the membrane interface. Other orientations might also behave in this way (Meister et al. 2006). Apart from that, no significant changes could be detected in the angle-dependent IRRAS measurements, within experimental accuracy, for the K-Ras4B proteins, which restricts detailed comparison with simulated spectra. Owing to the ambiguity in the generation of simulated IRRA spectra for the rather flexible GTP-loaded K-Ras4B molecules, detailed orientational information is not yet available (Dr I.R. Vetter, personal communication). However, our data indicate that K-Ras4B in the GDP-bound form interacts more strongly, on average, with the membrane with a preferred orientation, as indicated by the smaller fluctuations of the amide-I′ band maximum in IRRAS and the stronger negative dichroism

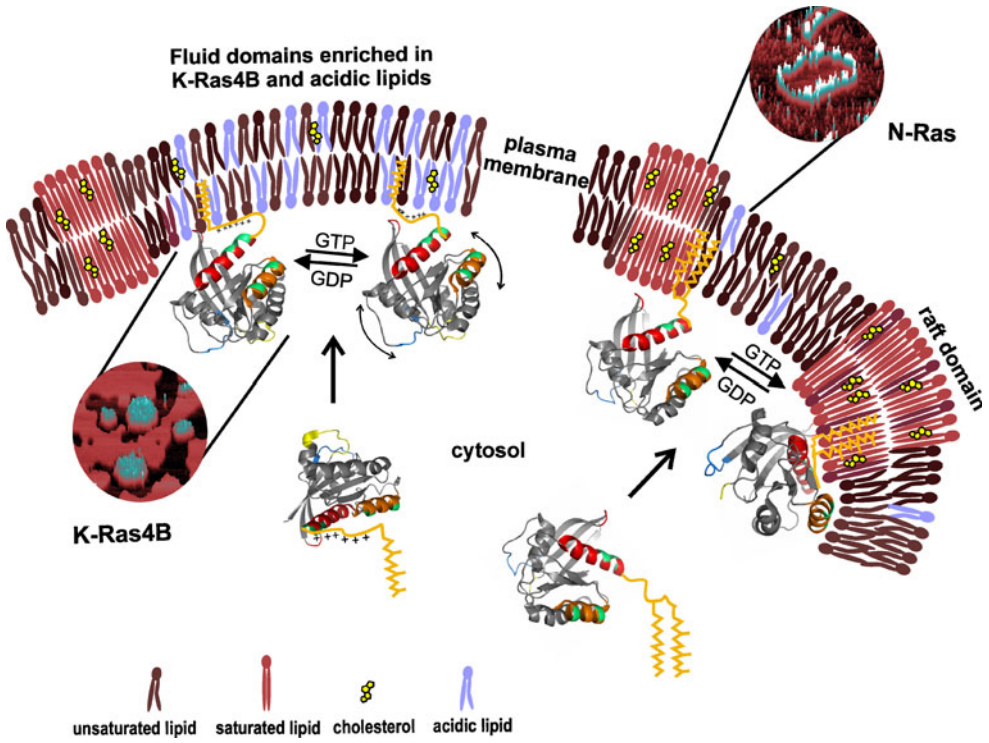

Fig. 7 This figure schematically summarizes the results obtained by use of a variety of biophysical techniques (confocal fluorescence microscopy, AFM, (ATR-)FTIR, IRRAS) for the Ras isoform-specific membrane interaction using heterogeneous model biomembranes (cf. Weise et al. 2009, 2011; Vogel et al. 2009; Kapoor et al. 2012). Ras proteins cluster in separate microdomains in the membrane, probably resulting in distinct signalling platforms (AFM detail with the clustered proteins depicted in *blue–white*). In addition, the G-domain mediates the Ras–membrane interaction by inducing different sets of preferred orientations in the active and inactive states. Thus, Ras-isoform specificity is further determined by different degrees of orientational flexibility for the active and inactive states of Ras, which may be important for isoform-specific effector interactions. Owing to the membrane-associated clustering of Ras proteins and intrinsic dynamics of the lateral organization and the lipid interface, no starkly fixed orientations are generally expected to prevail, rather different degrees of orientational fluctuations for the different Ras isoforms in their different nucleotide bound states. More or less average parallel orientation of most of the α-helices is envisaged for all Ras proteins. The images of the Ras G-domains were generated by use of PyMOL (PDB code: 3GFT for K-Ras4B and 3CON for N-Ras) with helices α4 and α5 depicted in *orange* and *red*, respectively

observed in the polarized ATR-FTIR data. A schematic diagram of the orientation of K-Ras4B GDP at membranes is depicted in Fig. 7, in which the protein orients with most of the helices parallel to the membrane interface and with its α5-helix toward the membrane, thus moving the G-domain close to the membrane. The reason for such a preferred orientation is based on corresponding FT-IR spectroscopy results (Weise et al. 2011) which show splitting of exclusively the α-helical subband to lower wavenumbers (indicative of stronger helix membrane interaction) upon membrane insertion. The presence of less pronounced dichroism for K-Ras4B in the active form (Fig. 3b) together with larger spectral shifts in IRRAS would imply that the protein spans a large set of orientations, leading to more randomized orientation. This is further supported by the similar membrane interaction behaviour observed for unlipidated K-Ras4B, with comparable spectral shifts, because of its inability to stably insert into membranes. The high orientational flexibility of K-Ras4B GTP revealed in this study is further supported by the recent findings by Lukman et al. (2010) of greater flexibility of the wild type active K-Ras compared with other Ras isoforms.

For N-Ras, the simulations revealed that the GDP-bound form is likely to adopt an average orientation in which the protein mainly interacts with the membrane through the HVR region and N-terminal residues (Kapoor et al. 2012). N-Ras GTP seems to have a different orientation (Fig. 7), in which nucleotide exchange triggers reorientation of the switch III (cf. Fig. 1), which is further coupled to the reorientation of the α4/5-helices, leading to pronounced interaction of these helices with the membrane. These results corroborate ATR-FTIR studies on bilayers in showing essentially parallel orientation of most of the helices relative to the membrane. Taken together, these results agree with the recently proposed balance model for Ras–membrane interactions in showing an inverted interaction profile for K-Ras compared with N-Ras (Gorfe et al. 2007b; Abankwa et al. 2008a, b). Thus, whereas interaction of the active conformation of N/H-Ras with the membrane is mediated by the α4/5-helices, K-Ras4B has greater flexibility in the active state, in which the α4-helix does not seem to directly interact with the membrane. The main conclusions drawn from these complementary data and simulations are summarized in Fig. 7 from which it can be stated that Ras isoform specificity extends beyond the HVR to the highly conserved G-domain, with different G-domain orientations of the Ras isoforms attuned by the bound nucleotide state and the HVR region.

Finally, with this study we add to the steady accumulation of evidence that the Ras isoforms are functionally distinct, in contrast with the earlier perception that they were essentially identical in function as oncoproteins. The distinct location for different isoforms, exposing them to different pools of effectors and regulators, coupled with the potential involvement of the homologous G-domain of Ras proteins in membrane orientation, suggests a synergy between this type of recognition motif and the specificity conferred by the HVR, thus validating the concept of isoform specificity in Ras.

Given that understanding of Ras signalling has increased substantially in recent years, the ability to selectively inhibit Ras isoforms has not yet kept pace. The area of search for the elusive "anti-Ras" drug is still emerging. As exemplified by this and previous studies focussed on the Ras–membrane interaction, an intriguing new level of complexity is evoked in the Ras conformational cycle. It is thus tempting to speculate that this might also apply to the oncogenic Ras conformations. Because it is known that effector proteins are able to sense the conformation and orientation of Ras, this information might be used in generating drug candidates that can target this conformational heterogeneity and thus specifically inhibit Ras–effector interactions and hence block oncogenic Ras signalling.

Acknowledgments This research was supported by the Deutsche Forschungsgemeinschaft (DFG, SFB 642) and the International Max Planck Research School (IMPRS). We are grateful to Christine Nowak for technical assistance. Furthermore, we thank Dr Andreas Kerth, Dr Annette Meister, and Professor Alfred Blume (all Martin-Luther-Universität Halle-Wittenberg, Germany) and Dr Andrea Gohlke for their help in setting up the IRRAS measurements in our laboratory. Finally, RW wants to thank Professor Dr Peter Laggner, to whom this work is dedicated, for many stimulating discussions in various fields of membrane biophysics over the years.

References

Abankwa D, Gorfe AA, Hancock JF (2008a) Mechanisms of Ras membrane organization and signalling: Ras on a rocker. Cell Cycle 7:2667–2673

Abankwa D, Hanzal-Bayer M, Ariotti N, Plowman SJ, Gorfe AA, Parton RG, McCammon JA, Hancock JF (2008b) A novel switch region regulates H-Ras membrane orientation and signal output. EMBO J 27:727–735

Abankwa D, Gorfe AA, Inder K, Hancock JF (2010) Ras membrane orientation and nanodomain localization generate isoform diversity. Proc Natl Acad Sci USA 107:1130–1135

Ausili A, Corbalan-Garcia S, Gomez-Fernandez JC, Marsh D (2011) Membrane docking of the C2 domain from protein kinase C alpha as seen by polarized ATR-IR. The role of PIP_2. Biochim Biophys Acta Biomembr 1808:684–695

Axelsen PH, Citra MJ (1996) Orientational order determination by internal reflection infrared spectroscopy. Prog Biophys Mol Biol 66:227–253

Bechinger B, Ruysschaert JM, Goormaghtigh E (1999) Membrane helix orientation from linear dichroism of infrared attenuated total reflection spectra. Biophys J 76:552–563

Bos JL (1989) Ras oncogenes in human cancer—a review. Cancer Res 49:4682–4689

Bringezu F, Majerowicz M, Wen SY, Reuther G, Tan KT, Kuhlmann J, Waldmann H, Huster D (2007) Membrane binding of a

lipidated N-Ras protein studied in lipid monolayers. Eur Biophys J 36:491–498
Brunsveld L, Kuhlmann J, Alexandrov K, Wittinghofer A, Goody RS, Waldmann H (2006) Lipidated Ras and Rab peptides and proteins—synthesis, structure, and function. Angew Chem Int Edit 45:6622–6646
Brunsveld L, Waldmann H, Huster D (2009) Membrane binding of lipidated Ras peptides and proteins: the structural point of view. Biochim Biophys Acta Biomembr 1788:273–288
Chen YX, Koch S, Uhlenbrock K, Weise K, Das D, Gremer L, Brunsveld L, Wittinghofer A, Winter R, Triola G, Waldmann H (2010) Synthesis of the Rheb and K-Ras4B GTPases. Angew Chem Int Edit 49:6090–6095
Evers F, Jeworrek C, Weise K, Tolan M, Winter R (2012) Detection of lipid raft domains in neutral and anionic Langmuir monolayers and bilayers of complex lipid composition. Soft Matter 8:2170–2175
Goormaghtigh E, Raussens V, Ruysschaert JM (1999) Attenuated total reflection infrared spectroscopy of proteins and lipids in biological membranes. Biochim Biophys Acta Rev Biomembr 1422:105–185
Gorfe AA, Babakhani A, McCammon JA (2007a) H-Ras protein in a bilayer: interaction and structure perturbation. J Am Chem Soc 129:12280–12286
Gorfe AA, Hanzal-Bayer M, Abankwa D, Hancock JF, McCammon JA (2007b) Structure and dynamics of the full-length lipid-modified H-Ras protein in a 1,2-dimyristoylglycero-3-phosphocholine bilayer. J Med Chem 50:674–684
Güldenhaupt J, Adiguzel Y, Kuhlmann J, Waldmann H, Kotting C, Gerwert K (2008) Secondary structure of lipidated Ras bound to a lipid bilayer. FEBS J 275:5910–5918
Hancock JF (2003) Ras proteins: different signals from different locations. Nat Rev Mol Cell Biol 4:373–384
Hancock JF, Parton RG (2005) Ras plasma membrane signalling platforms. Biochem J 389:1–11
Hancock JF, Paterson H, Marshall CJ (1990) A Polybasic domain or palmitoylation is required in addition to the Caax motif to localize p21 Ras to the plasma membrane. Cell 63:133–139
Hancock JF, Cadwallader K, Marshall CJ (1991) Methylation and proteolysis are essential for efficient membrane binding of prenylated p21 K-Ras(B). EMBO J 10:641–646
Harrick NJ (1967) Internal reflection spectroscopy. Interscience, New York
Huster D, Kuhn K, Kadereit D, Waldmann H, Arnold K (2001) H-1 high-resolution magic angle spinning NMR spectroscopy for the investigation of a Ras lipopeptide in a lipid membrane. Angew Chem Int Edit 40:1056–1058
Kapoor S, Werkmüller A, Denter C, Zhai Y, Markgraf J, Weise K, Opitz N, Winter R (2011) Temperature-pressure phase diagram of a heterogeneous anionic model biomembrane system: results from a combined calorimetry, spectroscopy and microscopy study. Biochim Biophys Acta Biomembr 1808:1187–1195
Kapoor S, Triola G, Vetter IR, Erlkamp M, Waldmann H, Winter R (2012) Revealing conformational substates of lipidated N-Ras protein by pressure modulation. Proc Natl Acad Sci USA 109:460–465
Karnoub AE, Weinberg RA (2008) Ras oncogenes: split personalities. Nat Rev Mol Cell Biol 9:517–531
Kuhn K, Owen DJ, Bader B, Wittinghofer A, Kuhlmann J, Waldmann H (2001) Synthesis of functional Ras lipoproteins and fluorescent derivatives. J Am Chem Soc 123:1023–1035
Lewis RN, McElhaney RN (1992) Structures of the subgel phases of n-saturated diacyl phosphatidylcholine bilayers: FTIR spectroscopic studies of $^{13}C{=}O$ and ^{2}H labeled lipids. Biophys J 61:63–77
Lukman S, Grant BJ, Gorfe AA, Grant GH, McCammon JA (2010) The distinct conformational dynamics of K-Ras and H-Ras A59G. PLoS Comput Biol 6:e1000922
Marsh D (1999) Quantitation of secondary structure in ATR infrared spectroscopy. Biophys J 77:2630–2637
Meister A, Nicolini C, Waldmann H, Kuhlmann J, Kerth A, Winter R, Blume A (2006) Insertion of lipidated Ras proteins into lipid monolayers studied by infrared reflection absorption spectroscopy (IRRAS). Biophys J 91:1388–1401
Mendelsohn R, Mao GR, Flach CR (2010) Infrared reflection-absorption spectroscopy: principles and applications to lipid–protein interaction in Langmuir films. Biochim Biophys Acta Biomembr 1798:788–800
Nagele E, Schelhaas M, Kuder N, Waldmann H (1998) Chemoenzymatic synthesis of N-Ras lipopeptides. J Am Chem Soc 120:6889–6902
Papahadjopoulos D, Vail WJ, Pangborn WA, Poste G (1976) Studies on membrane-fusion. 2. Induction of fusion in pure phospholipid membranes by calcium ions and other divalent metals. Biochim Biophys Acta 448:265–283
Prior IA, Muncke C, Parton RG, Hancock JF (2003) Direct visualization of Ras proteins in spatially distinct cell surface microdomains. J Cell Biol 160:165–170
Schubbert S, Bollag G, Shannon K (2007) Deregulated Ras signalling in developmental disorders: new tricks for an old dog. Curr Opin Genet Dev 17:15–22
Simons K, Toomre D (2000) Lipid rafts and signal transduction. Nat Rev Mol Cell Biol 1:31–39
Smith SO, Kustanovich I, Bhamidipati S, Salmon A, Hamilton JA (1992) Interfacial conformation of dipalmitoylglycerol and dipalmitoylphosphatidylcholine in phospholipid bilayers. Biochemistry 31:11660–11664
Tian TH, Harding A, Inder K, Plowman S, Parton RG, Hancock JF (2007) Plasma membrane nanoswitches generate high fidelity Ras signal transduction. Nat Cell Biol 9:905–960
Vogel A, Reuther G, Weise K, Triola G, Nikolaus J, Tan KT, Nowak C, Herrmann A, Waldmann H, Winter R, Huster D (2009) The lipid modifications of Ras that sense membrane environments and induce local enrichment. Angew Chem Int Edit 48:8784–8787
Waldmann V, Rabes HM (1996) What's new in ras genes? Physiological role of ras genes in signal transduction and significance of ras gene activation in tumorigenesis. Pathol Res Pract 192:883–891
Walsh AB, Bar-Sagi D (2001) Differential activation of the pac pathway by Ha-Ras and K-Ras. J Biol Chem 276:15609–15615
Weise K, Triola G, Brunsveld L, Waldmann H, Winter R (2009) Influence of the lipidation motif on the partitioning and association of N-Ras in model membrane subdomains. J Am Chem Soc 131:1557–1564
Weise K, Kapoor S, Denter C, Nikolaus J, Opitz N, Koch S, Triola G, Herrmann A, Waldmann H, Winter R (2011) Membrane-mediated induction and sorting of K-Ras microdomain signalling platforms. J Am Chem Soc 133:880–887
Willumsen BM, Christensen A, Hubbert NL, Papageorge AG, Lowy DR (1984) The p21 Ras C-terminus is required for transformation and membrane association. Nature 310:583–586
Wittebort RJ, Schmidt CF, Griffin RG (1981) Solid-state C-13 nuclear magnetic-resonance of the lecithin gel to liquid-crystalline phase-transition. Biochemistry 20:4223–4228
Wittinghofer A, Pai EF (1991) The structure of Ras protein—a model for a universal molecular switch. Trends Biochem Sci 16:382–387
Wittinghofer A, Waldmann H (2000) Ras—a molecular switch involved in tumor formation. Angew Chem Int Edit 39:4193–4214
Yan J, Roy S, Apolloni A, Lane A, Hancock JF (1998) Ras isoforms vary in their ability to activate Raf-1 and phosphoinositide 3-kinase. J Biol Chem 273:24052–24056
Zhai Y, Okoro L, Cooper A, Winter R (2011) Applications of pressure perturbation calorimetry in biophysical studies. Biophys Chem 156:13–23